Multi-stimuli Photo and Redox-active Nanostructured Mesoporous Silica Films on Transparent Electrodes

Samuel Ahoulou, Neus Vilà, Sébastien Pillet, Cédric Carteret, Dominik Schaniel, Alain Walcarius

Multi-stimuli Photo and Redox-active Nanostructured Mesoporous Silica Films on Transparent Electrodes

Samuel Ahoulou,[a,b] Neus Vilà,*[a] Sébastien Pillet,*[b] Cédric Carteret,[a] Dominik Schaniel,[b] and Alain Walcarius[a]

[a] Dr. S. Ahoulou, Dr. N. Vilà, Prof. C. Carteret, Prof. A. Walcarius
Université de Lorraine, CNRS
LCPME UMR 7564
54000 Nancy, France
E-mail: neus.vila@univ-lorraine.fr
[b] Dr. S. Pillet, Prof. D. Schaniel
Université de Lorraine
CRM2 UMR 7036
54000 Nancy, France
E-mail: sebastien.pillet@univ-lorraine.fr

Supporting information for this article is given via a link at the end of the document.

Abstract: Silica matrices hosting transition metal guest complexes may offer remarkable platforms for the development of advanced functional devices. We report here the elaboration of ordered and vertically oriented mesoporous silica thin films containing covalently attached tris(bipyridine)iron derivatives using a combination of electrochemically assisted self-assembly (EASA) method and Huisgen cycloaddition reaction. Such a versatile approach is primarily used to bind nitrogen-based chelating ligands such as (4-[(2-propyn-1-yloxy)]4'-methyl-2,2'-bypiridine, bpy') inside the nanochannels. Further derivatization of the bpy'-functionalized silica thin films is then achieved via a subsequent *in-situ* complexation step to generate $[Fe(bpy)_2(bpy')]^{2+}$ inside the mesopore channels. After giving spectroscopic evidences for the presence of such complexes in the functionalized film, electrochemistry is used to transform in a reversible way the confined diamagnetic (S=0) $\left[Fe_{LS}(bpy)_2(bpy')\right]^{2+}$ species to paramagnetic (S=1/2) oxidized $\left[Fe_{LS}(bpy)_2(bpy')\right]^{3+}$ species, while blue light irradiation (λ = 470 nm) enables to populate the short-lived paramagnetic (S=2) $\left[Fe_{HS}(bpy)_2(bpy')\right]^{2+}$ excited state. $[Fe(bpy)_2(bpy')]^{2+}$-functionalized ordered films are therefore both electro- and photo-active through the manipulation of the oxidation state and spin state of the confined complexes, paving the way for their integration in optoelectronic devices.

Introduction

Recent advances in the field of nanotechnology, especially nanoelectronics, sensors or bioelectronics, have sustained the need for versatile and processable materials whose properties can be easily tailored and fine-tuned at the nanoscale. In that context, hybrid organic-inorganic materials based on inorganic porous matrices hosting organic functional components exhibit attractive properties resulting from the coupling at the molecular level of the inorganic and organic elements in one single material.[1-3] Porous silica is a relevant host candidate as such inorganic matrix offers appealing characteristics, such as thermal stability, mechanical robustness, optical transparency and electrical insulation. The mesostructure of the inorganic matrix (porosity, architecture and spatial arrangement) can be adjusted to the specific need by the use of sol gel chemistry, combined with the appropriate use of structure-directing agents (surfactants or amphiphilic block copolymers) through a self-assembly process.[4]

Among various morphologies (nanoparticles, monoliths, films), mesoporous silica thin films deposited on flat substrate are favourable for practical applications and device fabrication.[5-7] Ordered and unidirectionally oriented mesoporous silica offers advantages with respect to non-ordered silica, resulting from the larger surface area and better pore accessibility.[8,9] With that respect, two main chemical solution deposition routes have been proposed in the literature to generate mesoporous silica thin films: the solvent evaporation induced self-assembly (EISA),[10,11] and the electrochemically assisted self-assembly (EASA).[12-15] The EISA method consists in casting the coating sol containing amphiphilic surfactant templates on the surface of a specific substrate, while the evaporation process is controlled. It results in mesoporous silica films with various pore structures,[10] but those based on 1D aligned mesochannels are mostly oriented parallel to the surface and thus less accessible to external reagents.[16-17] To render this material more appropriate for electrochemical applications and electrochemical processing (enhanced accessibility of the pores, faster electron transfer processes, easy mass transport of the electroactive species and interfacial contact between the redox active confined guest and the electrolyte), the design of practical silica-based films with a vertical orientation of the nanochannels is desired. In this sense, the EASA strategy consists in the concomitant electrochemically induced self-assembly of surfactant and silica thin film growth.[12,13] It leads to vertically oriented and ordered silica films on semi-conducting or conducting substrates (fluorine-doped tin oxide (FTP), indium-tin oxide (ITO), carbon, gold, copper).[15]

Various methods are available to incorporate organic functionalities into porous inorganic matrices, mainly based on post-synthesis grafting and the co-condensation approaches, resulting in molecular fragments covalently attached to the silica framework[,14] these strategies can be also applied to the functionalization of mesoporous silica thin films.[18] Both methods have their respective advantages and drawbacks, the most significant advantage of the co-condensation method over the grafting one being the uniform spatial distribution of organic groups within the mesoporous silica materials and higher loading of organic functionalities. They are however not suitable

for the functionalization of vertically-oriented mesoporous silica thin films obtained by EASA (pore blocking, lack of mesostructural order), for which an alternative method has been proposed, dealing with the use of the Cu(I)-catalyzed azide alkyne cycloaddition (CuAAC) or other click reactions,[15,16] resulting in numerous functionalized films.[19-22] Alternatively, target molecules can be easily confined in mesoporous silica matrices by host-guest chemistry, i.e. by immersion of the silica film in a solution of the dopant molecule, enabling its attachment through hydrogen bonds or electrostatic interactions. Following these strategies, numerous ordered hybrid nanocomposites have been designed by confining or grafting appropriate molecules for energy,[23-25] luminescent,[26-29] optoelectronic,[30] or electrochemical devices.[31] In addition, the perfect 1D orientation of the nanochannels, whether they are oriented parallel or perpendicular to the supporting surface, can allow an alignment or 1D growth of anisotropic nanowires or nanorods, leading ultimately to a desired anisotropy in the resulting physical properties.[32-37] More recently, a composite mesoporous material based on $Fe(Htrz)_3@SiO_2$ has been obtained in one pot, evidencing a template role of the spin crossover $Fe(Htrz)_3$ coordination polymer itself during the thin film growth.[38] The importance of having periodic ordered mesoporosity is highlighted for instance by the improved performance of $Ru(bpy)_3$-containing silica nanocomposites for photovoltaic and chemiluminescence processes, resulting from an efficient charge transfer to the supporting electrode and better contacts with the hole-transporting electrolyte in such ordered materials.[39]

Owing to their unique chemical, photochemical, and photophysical properties (luminescence emission, long-lived charge transfer excited states, redox activity in both the ground and excited states), transition metal complexes offer great possibilities in designing functional hybrid materials. They exhibit rich metal-based redox processes, together with a large variety in electronic configurations and excited-state dynamics, which have made transition metal complexes excellent candidates for interconversion between light, chemical, and electrical energies. Especially polypyridine coordination complexes (of Ru^{2+}, Os^{2+}, Ir^{2+}, Re^{+}, Cu^{+}) are used in a large variety of applications such as electrochemiluminescence cells [39,24], dye-sensitized solar cells,[40] (DSSC), light-emitting diodes,[41] photocatalysis,[42,36] or redox flow batteries.[43,44] In contrast with $Ru(bpy)_3^{2+}$ chromophore , a well-known photosensitizer characterized by its long-lived metal-to-ligand charge-transfer (MLCT) excited-state, Fe-polypyridine complexes show a much faster deactivation of the ^{3}MLCT states to non-emissive low-lying metal-centered states, inappropriate for efficient photosensitizers. The $[Fe(bpy)_3]^{2+}$ complex is known to be a low spin (LS) system with a high-spin (HS) to LS energy difference ΔE^0_{HL} of nearly 6000 cm^{-1}, and hence does not undergo a thermal spin crossover. The LS to HS conversion can nevertheless be optically triggered by the LIESST ("Light Induced Excited Spin State Trapping") process.[45-48] The light-induced excited-state dynamics of the $[Fe(bpy)_3]^{2+}$ chromophore in solution is well established from pump-probe X-ray scattering and X-ray absorption spectroscopy[49-52] and UV-visible absorption spectroscopy experiments.[53-61] The conversion from the LS (S=0) to the HS (S=2) state occurs in less than 1 ps with a quantum efficiency of nearly 1.[62] The general mechanism consists in a light-induced $^1A_1 \rightarrow {}^1$MLCT transition, followed by two successive intersystem crossings to the metal centered quintet $^5T_2$ high-spin state, through the intermediate ^{3}MLCT state (or ^{3}MC state, there is still controversy on that subject): $^1A_1 \rightarrow {}^1MLCT \rightarrow {}^3MLCT \rightarrow {}^5T_2$. The intersystem crossing within the singlet and triplet MLCT manifold occurs in less than 30 fs, while the transition and vibrational cooling in the quintet potential requires nearly 150 fs.[49,50,52,56] The HS state relaxes non radiatively to the GS in less than 700 ps. Unlike its Ru counterpart, $[Fe(bpy)_3]^{2+}$ is not appropriate as photosensitizer owing to its fast deactivation to the metal centered quintet HS state, but on the contrary, it can be very useful for fast magneto-optic devices, using light as a single control stimulus. As such, many photochromic, electrochromic, or photomagnetic materials, for which the physical properties (electrical, optical, magnetic) can be controlled by an appropriate external perturbation, have been reported.[63-65] However, reaching a physical control with two different external stimuli (e.g. electrochemical control and photochemical control) still remains a very delicate and challenging task.

Recently, the combination of the EASA method and the Huisgen cycloaddition reaction has been exploited to fabricate nanostructured vertically-oriented silica thin films based on $Fe(tpy)_2$ exhibiting electrochromic properties. In this sense, the preliminary results have demonstrated the feasibility of this approach consisting in the elaboration of electrochromic thin films.[66] The elaborated film is switchable using a single external stimulus. With that respect, we propose in the present manuscript to push forward this strategy and to immobilize the $[Fe(bpy)_3]^{2+}$ chromophoric units, which has the potential to switch using two different stimuli (redox and photo-induced), therefore adding the photoswitching functionality. $[Fe(bpy)_3]^{2+}$ chromophores have been confined within a mesoporous ordered silica thin film whose nanochannels are oriented perpendicular to the supporting ITO electrode. The approach is based on the simple and versatile strategy combining electro-assisted self-assembly (EASA) and click-chemistry to functionalize the inner nanochannels with bpy-type pendent ligands, which are then used to trigger the formation and fixation of the $[Fe(bpy)_3]^{2+}$ entities (rigorously speaking $[Fe(bpy)_2(bpy')]^{2+}$, vide supra). The main goal of this work is to use electro- and photo-stimulations to control the valence state and spin state of the confined $[Fe(bpy)_3]^{2+}$ entities, opening the way for the development of electrochemically and optically driven magnetic films, with possible applications of such ordered and periodic organo-silica films in smart optical devices.

Results and Discussion

Immobilization of $[Fe(bpy)_2(bpy')]^{2+}$ species in the mesoporous silica films

EASA is first applied to the self-assembly co-condensation of an alkoxysilane (namely tetraethoxysilane, TEOS) and an organo-alkoxysilane (namely 3-azidopropyltriethoxysilane, Az-PTES) in the presence of CTAB as surfactant template to elaborate azido-functionalized ordered and vertically aligned silica films on ITO.[19] Such films containing homogeneously distributed azidopropyl functions can be used to further attach various alkyne-bearing molecules by exploiting the Cu(I)-catalyzed azide alkyne cycloaddition (CuAAC).[19-22] Here, we made use of this

reaction to immobilize a bipyridine derivative (the 4-[(2-propyn-1-yloxy)]4'-methyl-2,2'-bypiridine, denoted bpy') in the mesopore channels, and to use it afterwards as the basis for the formation of the $[Fe(bpy)_2(bpy')]^{2+}$ complex in the mesoporous films. The effectiveness and completion of all steps of the sequential synthesis (scheme 1) have been characterized by means of various physico-chemical techniques.

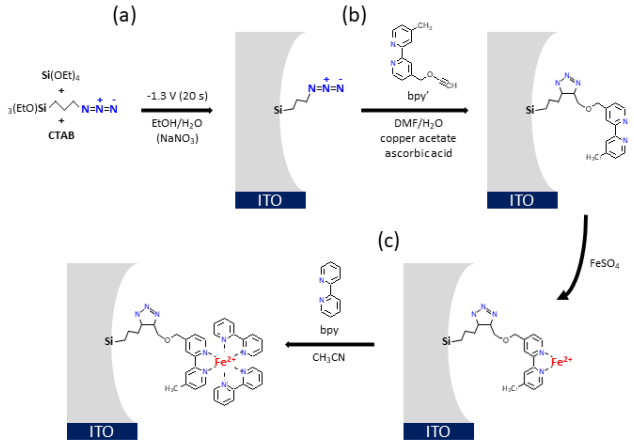

Scheme 1. Strategy for the confinement of $[Fe(bpy)_2(bpy')]^{2+}$ moieties within ordered mesoporous silica thin films: (a) generation of azido-functionalized silica material; (b) click coupling with an ethynyl bipyridine derivative (bpy'); (c) complexation with Fe^{2+} and 2,2'-bipyridine (bpy).

Infrared spectroscopy characterization

The click coupling of the azido-functionalized silica film with bpy' was first evaluated (at the semi-quantitative level) using infrared spectroscopy (Fig. S1). The spectra corresponding to the azido-functionalized sample exhibits characteristic features of silica: a strong vibration band at 1080 cm^{-1} and a well resolved shoulder at 1229 cm^{-1} corresponding to the asymmetric stretching of the Si-O-Si network (referred in the literature as the transverse optic TO, and longitudinal optic LO phonon components of the in-plane and out-of-plane modes).[67,68] The vibration band at 960 cm^{-1} is typical of Si-OH stretching vibrations, confirming the presence of silanol groups in the film, while the observed 808 cm^{-1} band involves rocking vibration of Si-O-Si bridges. The vibration band at 2100 cm^{-1} corresponds to the asymmetric stretching vibration of the azido group ($\nu_{asym}(N_3)$), the corresponding symmetric stretching mode is expected much weaker and overlapping with the Si-O-Si stretching vibration.[69] After coupling of the azido group with the {(4-[(2-propyn-1-yloxy)]-4'-methyl-2,2'-bipyridine)} (bpy') via the Huisgen click reaction, the IR spectra shows a decrease of the 2100 cm^{-1} azido stretching vibration band, together with the apparition of a new band at 1656 cm^{-1}. This latter is attributed to the stretching vibration modes of the C=C and C=N bonds of the triazole ring formed during the click reaction and bipyridine moieties attached.

Complex formation and film permeability characterization

The bpy' functionalized films were further dipped in a 10 mM $FeSO_4$ aqueous solution under nitrogen atmosphere, followed by washing with acetonitrile, and dipped into an acetonitrile solution of 30 mM bpy. The films turned immediately pink, which reveals the *in situ* formation of $[Fe(bpy)_2(bpy')]^{2+}$. Another, yet indirect, way to evidence the presence of $[Fe(bpy)_2(bpy')]^{2+}$ within the channels is through the characterization of the film permeability. This has been performed by cyclic voltammetry using $Fc(MeOH)_2$ as a redox probe in solution (Fig. S2). For an ITO electrode covered with an unmodified oriented mesoporous silica film, the voltammetry shows well-defined reversible signals corresponding to the $Fc(MeOH)_2^+/Fc(MeOH)_2$ system around +0.24 V vs. Ag/AgCl. For the AzPTES-functionalized film, a similar signal appears at the same potentials, with nonetheless decreased peak currents due to the presence of azidopropyl groups contributing to slow down mass transport of the probe through the mesopore channels. The same situation holds for the $[Fe(bpy)_2(bpy')]^{2+}$-functionalized films with a slight potential shift to +0.26 V and even more decreased peak currents because of the presence of the bulkier $[Fe(bpy)_2(bpy')]^{2+}$ moieties in the mesopores. This suggests the successful functionalization steps and indicates that the functionalized films remain permeable to the $Fc(MeOH)_2$ probe, yet with some restricted diffusion rates due to the presence of the pendent groups covalently attached to the mesopore surface.

Raman spectroscopy characterization

In order to confirm the nature of the attached $[Fe(bpy)_2(bpy')]^{2+}$ species, and detect a possible change of Fe valency or spin state resulting from their confinement and attachment to the silica walls, resonance Raman spectra have been recorded (Fig. 1) under excitation into the metal(d)→bpy(π^*) metal-to-ligand charge transfer (MLCT) absorption band (λ_{ex} = 532 nm). In such conditions, Raman scattering is enhanced for totally symmetric vibration modes which couple the ground state and MLCT excited state of $[Fe(bpy)_2(bpy')]^{2+}$, and therefore are vibronically active in the corresponding electronic transition. A clear assignment of all the Raman active and infrared active vibrational bands has been provided for $[Fe(bpy)_3]^{2+}$ and $[Ru(bpy)_3]^{2+}$ from resonant Raman, infrared, and DFT calculations.[70-75]

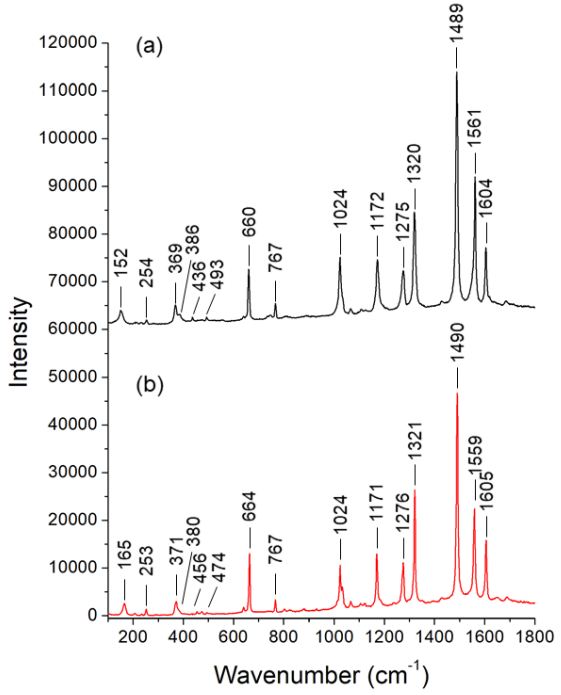

Figure 1. Resonance Raman spectra at an excitation wavelength of 532 nm of (a) $[Fe(bpy)_2(bpy')]^{2+}$-functionalized mesoporous silica film and (b) reference $[Fe(bpy)_3]SO_4.7.5H_2O$ microcrystalline powder.

The Raman spectra measured for the $[Fe(bpy)_2(bpy')]^{2+}$-functionalized film and $[Fe(bpy)_3]SO_4.7.5H_2O$ microcrystalline powder used as a reference are given respectively in parts (a) and (b) of figure 1. In the microcrystalline powder, the structure adopts a *C2/c* space group, with the $[Fe(bpy)_3]^{2+}$ molecule sitting on a general position with point group 1.[76] Although the ideal symmetry of solvated $[Fe(bpy)_3]^{2+}$ (or similarly $[Ru(bpy)_3]^{2+}$) species is D_3, time-resolved resonance Raman experiments have shown that for the $[Ru(bpy)_3]^{2+}$ complex, the MLCT state can be formulated as $[Ru^{3+}(bpy^0)_2(bpy^-)]^{2+}$ with the transferred electron localized on one of the three equivalent bpy ligand on the vibrational time scale, leading to a maximum symmetry of C_2.[70,77,78] An inspection of the vibration modes for the thin film shows close similarities with that of the microcrystalline powder and matches nicely those reported in the literature for solutions, adsorbed species and similar solid salts.[73,77-81] The confined $[Fe(bpy)_2(bpy')]$ complex is therefore most probably in a 2+ formal charge, and retains a high symmetry. In particular, the 600-1650 cm^{-1} spectral range, corresponding to the skeleton vibration modes (in-plane and out-of-plane ring deformations and ring stretching modes of bpy) of the coordinated bipyridine ligands does not present any splitting or significant frequency shift (less than 2 cm^{-1}). This is expected since these modes are almost insensitive to the distortion of the FeN_6 coordination environment. Especially the ring stretching mode with a strong C=C and C=N component at 1604 cm^{-1}, which is considered as the most active in the vibronic coupling, does not exhibit any frequency shift. The 100-600 cm^{-1} low frequency range exhibits several weak vibration modes characteristic of the $[Fe(bpy)_3]$ coordination, which can be used as signatures of a possible distortion of the coordination sphere. The bands at 372 and 380 cm^{-1} are related to the Fe-N stretching vibration. The band at 165 cm^{-1} has already been observed for non-coordinated[82] as well as coordinated bpy ligands, showing some metal (Fe, Ni, Zn) and counter ion (I^-, BF_4^-, ClO_4^-) frequency variability in the range 161-173 cm^{-1}.[77,83] A significant shift from 165 cm^{-1} to 152 cm^{-1} is observed for this band in the silica matrix, which may possibly originate from the confined solvated environment. The high frequency region 1600-3200 cm^{-1} shows clear and distinct overtones and combination bands (Fig. S3), both in the functionalized film and the microcrystalline powder, with no significant frequency shifts. The strong similarity between the microcrystalline powder and the functionalized-film spectra confirms the nature of the confined species as $[Fe(bpy)_2(bpy')]^{2+}$.

Concerning the exact Fe oxidation state and spin state, the skeleton vibration modes are only slightly sensitive to the Fe spin state owing to a modification of the π-back bonding Fe-bpy interaction between the LS ($^1A_1$) and HS ($^5T_2$) states, thus modifying the π-electron distribution on the bpy ligand. It has been shown for the related poly-pyridyl spin crossover complexes $[Fe(phen)_2(NCS)_2]$ and $[Fe(bpy)_2(NCS)_2]$ that the Fe-N stretching vibration is extremely sensitive to the Fe^{2+} spin state, with a 150 cm^{-1} frequency shift from the LS ($^1A_1$) to HS ($^5T_2$) state, from 368-376 cm^{-1} to 220-252 cm^{-1} for $[Fe(phen)_2(NCS)_2]$, and from 384 cm^{-1} to 235 cm^{-1} for $[Fe(bpy)_2(NCS)_2]$.[84-89] This frequency shift is the signature of the large structural reorganization of the FeN_6 coordination environment upon the spin transition ($\Delta d_{Fe\text{-}N(bpy)}$ ~ 0.207 Å for $[Fe(bpy)_2(NCS)_2]$) as characterized by X-ray crystallography[89]), and therefore strong modification of the Fe-N bond strength. On the contrary, a moderate shift by 2 cm^{-1} has been reported for a change of oxidation state from Fe^{3+} to Fe^{2+} comparing $[Fe(bpy)_3](ClO_4)_3$ to $[Fe(bpy)_3](ClO_4)_2$.[83] The 372 and 380 cm^{-1} vibration bands in the functionalized-film confirm therefore the oxidation state and spin state of the confined species as LS $[Fe(bpy)_2(bpy')]^{2+}$. The in-plane ring deformation of bipyridine is also very sensitive to the spin state, shifting from 624 cm^{-1} to 496 cm^{-1} upon the HS ($^5T_2$) to LS ($^1A_1$) transition in $[Fe(bpy)_2(NCS)_2]$.[86] By comparison, the corresponding position at 493 cm^{-1} and 474 cm^{-1} for the functionalized-film and microcrystalline powder is also consistent with the LS state.

Altogether, the resonance Raman spectroscopic results show that the confined attached species are indeed $[Fe(bpy)_2(bpy')]$ in the formal 2+ oxidation state, and LS state.

XPS characterization

X-ray photoelectron spectroscopy (XPS) yields spectra with the binding energy specific of the corresponding chemical and local environment of the considered atom. In the present context, XPS has been used to characterize the sequential formation of the $[Fe(bpy)_2(bpy')]^{2+}$ complex within the nanochannels and to confirm further the nature of confined species. XPS survey spectrum shows the presence of C1s, O1s, N1s, Si2p and Fe2p signals. Analysis and discussion of the XPS spectra is mainly focused in the N1s core level region before and after the click reaction allowing the incorporation of bpy' ligands within the nanopores and later on the Fe2p region after *in situ* formation of the $[Fe(bpy)_2(bpy')]^{2+}$ complex (Fig. S4 and Fig. S5). Azide-functionalized films shows two major components (2:1 ratio) at the N1s core level, located at 400.6 eV and 404.2 eV (Fig. S4A1), which can be respectively attributed to electron-rich and electron-poor azide nitrogen atoms. Upon incorporation of bpy'

ligands via Huisgen cycloaddition reaction, the peak at high binding energies characteristic of the central nitrogen in the azide functions is absent and two distinct peaks at 401.7 eV and 400.9 eV (Fig. S4A2) characteristic of the triazole moieties are observed. Upon coordination with Fe^{2+}, the binding energy of the N1s peak located at 400.9 eV for the bpy'-functionalized films shifted to 399.9 eV (Fig. S4A3). The binding energies of the Fe 2p core level in the $[Fe(bpy)_2(bpy')]^{2+}$-functionalized films are in good agreement with the literature (Fig. S5) and, as expected, no signal for Fe can be observed before complex formation.[90] The XPS analysis revealed that the calculated atomic ratio of N/Fe was 5.6, which is close to the atomic ratio of the reference complex (N/Fe ~ 6:1), suggesting the quantitative formation of tris(2,2′- bipyridine)−Fe^{2+} complexes inside the mesochannels.

Film structure

As shown by transmission electron microscopy (TEM, Fig. 2), the $[Fe(bpy)_2(bpy')]^{2+}$-functionalized thin films exhibit a hexagonal packing of the mesopores over large surface area, very similar to the non-functionalized EASA-based mesoporous silica films,[12] indicating that the successive functionalization steps did not result in any mesostructural order lost. The cross-section view (Fig. 2A) confirms the vertical alignment of the mesochannels through the membrane, with a measured uniform thickness of nearly 100 nm. The center-to-center distance between adjacent mesopores identified on the cross-section and the top view corresponds to a d-spacing of 4.2 nm, in agreement with previous observations made on similar films functionalized with other groups.[19] The hexagonal ordering is further highlighted by the calculated Fast Fourier Transform (FFT) images in the left insert of figure 2B.

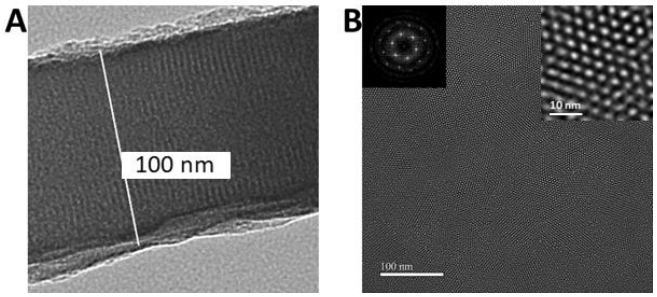

Figure 2. TEM images of the electrodeposited $[Fe(bpy)_2(bpy')]^{2+}$-functionalized films: (A) Cross-sectional view; (B) Top view. The inserts depict a zoom on the top view (right) and the calculated Fast Fourier Transform (left).

Electrochemical response of the $[Fe(bpy)_2(bpy')]^{2+}$-functionalized films

Cyclic voltammograms (CV) of the $[Fe(bpy)_2(bpy')]$-functionalized films recorded in aqueous medium with $NaNO_3$ as supporting electrolyte (Fig. 3) revealed a reversible one-electron transfer signal located at $E_{1/2}$=+0.87 V vs Ag/AgCl ($E_{1/2} = \frac{(E_p^a + E_p^c)}{2}$), similarly to what was observed for $[Fe(bpy)_3]^{2+}$ in the same solution on bare ITO electrode (Fig. S6). This demonstrates that $[Fe(bpy)_2(bpy')]^{2+}$ complexes covalently immobilized in the mesoporous film are electrochemically accessible and behave similarly to the structurally related $[Fe(bpy)_3]^{2+}$ species in solution. When operating at various potential scan rates from 10 mV s^{-1} to 100 mV s^{-1} (Fig. 3A), it appeared that the difference between the anodic and cathodic peak potentials, $\Delta E_p = E_p^a - E_p^c$, increased from 115 mV to 175 mV, suggesting some resistance to charge transfer. ΔE_p values were however lower than for $[Fe(bpy)_3]^{2+}$ on bare ITO, indicating some stabilization effect of the mesoporous silica host. Upon multiple successive potential scanning (Fig. 3B), after some decrease in intensity during the first 10 cycles, the voltammetric signals reached a steady-state value, supporting the operational stability of the system. Within the potential window accessible for ITO in aqueous medium, only the metal-centered one-electron oxidation of the diamagnetic (S=0) dicationic complex to the low spin (S=1/2) tricationic complex is possible, without any chance to see eventual ligand-centered reduction processes as those likely to occur in dry organic solvents.[91]

From the integration of the peak currents, and given the surface of the film deposited on the electrode, one can estimate a surface concentration of 5.9×10^{-9} mol.cm^{-2} $[Fe(bpy)_2(bpy')]^{2+}$ in the film, which is much more than a monolayer onto the ITO area. It means that the electron transfer mechanism involved in such $[Fe(bpy)_2(bpy')]^{2+}$-functionalized silica thin films is the electron hopping between adjacent redox sites and simultaneous transport of electrolyte anions (NO_3^-) through the film to maintain charge balance (i.e., ingress of anions to compensate the positive charges generated by the oxidation of $[Fe(bpy)_2(bpy')]^{2+}$ moieties). As a result, these processes are diffusion-controlled, as pointed out by the linear variation of the peak currents as a function of the square root of potential scan rates[92] (see inset in Fig. 3A). This behavior is similar to the ferrocene functionalized mesoporous silica films reported previously.[93]

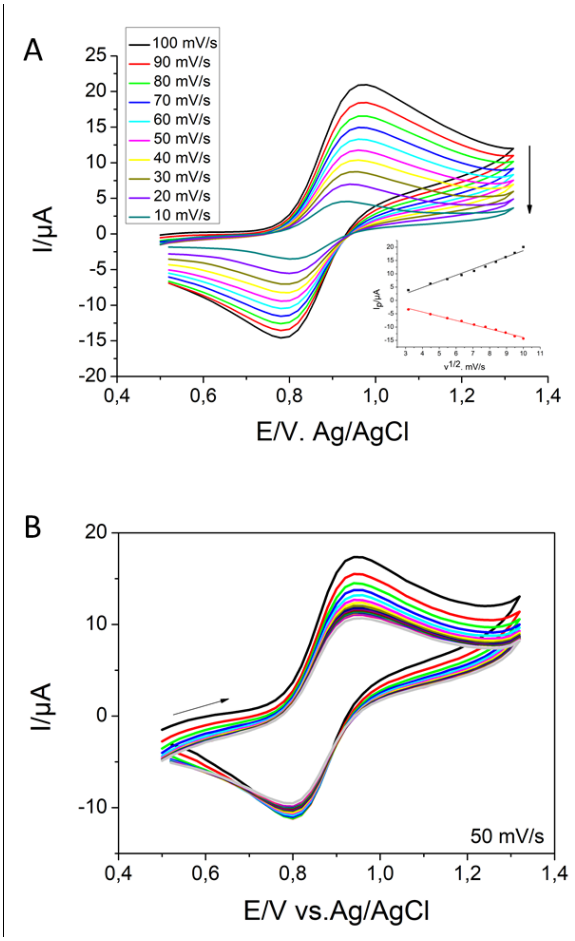

Figure 3. (A) CV curves recorded at increasing potential scan rates (10-100 mV s^{-1}) for $[Fe(bpy)_2(bpy')]^{2+}$-functionalized mesoporous silica film in aqueous solution containing 0.1 M $NaNO_3$; inset: corresponding variations of peak currents as a function of the square root of scan rate. (B) 20 consecutive CVs recorded at 50mV s^{-1} using the same electrode in the same medium as in (A).

Altogether, these electrochemical results show that the functionalized thin films exhibit quite stable and reversible one-electron redox switching between $[Fe(bpy)_2(bpy')]^{2+}$ and $[Fe(bpy)_2(bpy')]^{3+}$ functions.

Optical functionalities of the $[Fe(bpy)_2(bpy')]^{2+}$-functionalized films

Electronic absorption spectroscopy has been used to monitor the optical properties of the $[Fe(bpy)_2(bpy')]^{2+}$-functionalized silica thin film. The photophysical properties of $[Fe(bpy)_3]^{2+}$ (as well as $[Ru(bpy)_3]^{2+}$ and $[Os(bpy)_3]^{2+}$) have been extensively studied in solution,[94-96] crystalline phase, [97-100] or doped into isostructural host crystalline matrices $[M(bpy)_3](PF_6)_2$ with M=Co, Zn, Cd, or Mn.[45-47, 101] The assignment of the observed absorption bands has been proposed with respect to Molecular Orbital calculations and energy diagram determination.[101-103]

The optical absorption spectrum measured on our $[Fe(bpy)_2(bpy')]^{2+}$-functionalized silica thin film is compared with that of an aqueous solution containing 2 mM $[Fe(bpy)_3]^{2+}$ (Fig. S7). While $[Fe(bpy)_3]^{2+}$ ions in solution should exhibit the ideal D_3 point group symmetry, the $[Fe(bpy)_2(bpy')]^{2+}$ cations covalently confined in the film may suffer from structural distortions, modifying the corresponding energy diagram and optical transitions. The spectrum corresponding to $[Fe(bpy)_3]^{2+}$ in solution consists of intense low-lying bands centered around 520 nm (19230 cm^{-1}) and 350 nm (28570 cm^{-1}), which are assigned to spin allowed Metal-to-Ligand Charge Transfer (^{1}MLCT) transitions from Fe(3d) orbitals to π^* bipyridine ligand orbitals. Each band consists of a principal band of higher intensity and a weaker well-defined shoulder on the high-energy side for the 520 nm absorption, and on the low-energy side for the 350 nm absorption, the peak to shoulder separation is close to 1624 cm^{-1}, which corresponds to a ring stretching vibration mode identified in the resonance Raman analysis. The splitting of the two absorption bands may result in each case from a vibronic structure of the single MLCT excitation or, alternatively, from several distinct charge transfer excitation transitions. We have fitted the main ^{1}MLCT region centered at 520 nm of the absorption spectrum using a single-mode vibrational progression (see Fig. S8 and details in SI), leading to a Huang-Rys parameter of S=0.778(8) and ν_{vib} = 1624(9) cm^{-1}, in good agreement with our Raman study. These values are furthermore consistent with those derived for the related $[Ru(bpy)_3]^{2+}$ compound in solution[57] or in $[Ru(bpy)_3](PF_6)_2$ single crystals through polarized optical absorption measurements[104], although the derived vibrational frequency is higher than those obtained in a similar experiment on $[Fe(bpy)_3]^{2+}$ by Gawelda *et al*. (ν_{vib} = 1607 cm^{-1}).[56] Our model adjustment indicates also the presence of weak spin forbidden ^{3}MLCT bands, detected as a tail around 16000 cm^{-1} in the low frequency side of the ^{1}MLCT band. On the contrary, weak dipole-forbidden Fe(d-d) ligand field transitions are not detected in our measurement; these are obscured by the strong ^{1}MLCT band in the visible range. The UV part of the spectrum (below 320 nm) is dominated by the strong intraligand π-π^* transitions.

The absorption spectrum measured for the $[Fe(bpy)_2(bpy')]^{2+}$-functionalized silica film is very similar to that of $[Fe(bpy)_3]^{2+}$ in solution (compare the two curves in Fig. S7). We note that the peak resolution is nevertheless lower due to the superimposed strong background originating from the mesoporous silica scattering signal, which is quite intense in the UV part of the spectrum. The strong similarity with the absorption spectrum of $[Fe(bpy)_3]^{2+}$ confirms the tris(2,2'-bipyridine)iron(II) type coordination within the silica films, and shows that the functionalization of one bipyridine ligand by the click-chemistry process (bpy→bpy') barely modify the energy diagram of the entrapped $[Fe(bpy)_2(bpy')]^{2+}$ complex. Especially the ^{1}MLCT absorption bands at 520 nm and 350 nm exhibit the characteristic shoulder owing to the vibronic coupling which is effective in the silica film, and is not affected by confinement. We therefore might expect that the whole photophysical properties are preserved.

Spectroelectrochemical response of the $[Fe(bpy)_2(bpy')]^{2+}$-functionalized films

It is well known that a change of oxidation state in a transition metal complex results in a strong modification of the electronic structure and may induce charge redistribution. As a consequence, for redox active and stable complexes, the redox control offers an attractive possibility to tune the electronic, and

as a consequence, the optical properties of the considered complex. Spectroelectrochemical measurements can provide important information on the coupling between redox and spectroscopic behaviors, combining energetic and mechanistic information from electrochemistry to spectroscopic signatures of the electrogenerated species.

We have detailed above the redox and spectroscopic behaviors of our $[Fe(bpy)_2(bpy')]^{2+}$-functionalized thin films. The electrochemical results from cyclic voltammetry showed a reversible one-electron metal-centered oxidation-reduction wave of the Fe^{2+}/Fe^{3+} couple. The UV-vis absorption spectra of 0.1 mM aqueous solutions of $[Fe(bpy)_3]^{2+}$ and $[Fe(bpy)_3]^{3+}$, which would correspond to the reduced and oxidized species of the $Fe(bpy)_3^{2+/3+}$ couple, have been measured, and will be used as benchmarks for the spectro-electrochemical study (Fig. S9). The $[Fe(bpy)_3]^{2+}$ absorption spectrum is dominated by the intense MLCT ($t_{2g}\rightarrow\pi^*$) absorption transitions with maximum at 520 nm, while for the oxidized $[Fe(bpy)_3]^{3+}$ species, the charge transfer takes place from the ligand to the metal $\pi\rightarrow t_{2g}$ (LMCT) and the maximum occurs at 627 nm (barely detectable) with a molar absorptivity more than one order of magnitude lower than for the dicationic $[Fe(bpy)_3]^{2+}$ counterpart.[105-108] As a consequence, if this contrast is confirmed for the functionalized films, this would offer the possibility of an electrochromic response, associated with an electronic oxidation/reduction of the confined Fe complex. In other words, the film could be considered as an optical device controlled by an external current or potential.

In order to verify this functionality, we have monitored the evolution of the UV-vis electronic absorption spectrum as a function of applied potential using a homemade spectro-electrochemical cell. The thin film sample was placed in a quartz cuvette containing 0.05M NBu_4BF_4 as supporting electrolyte and an Ag/AgCl reference electrode. Then a potential of +1.3V (higher than the measured $[Fe(bpy)_2(bpy')]^{2+}/[Fe(bpy)_2(bpy')]^{3+}$ oxidation wave) was applied to the working electrode for 1000s, and the UV-vis absorption spectrum has been recorded as a function of time. The results are given in figure 4. We can see a progressive decrease, yet slight, of the absorption centered at 525 nm, which corresponds to a progressive attenuation of the MLCT absorption band of the $[Fe(bpy)_2(bpy')]^{2+}$ species. This is due to a partial $Fe^{2+}\rightarrow Fe^{3+}$ oxidation of the confined $[Fe(bpy)_2(bpy')]$ species. As a result of the electrochemical reversibility of the $[Fe(bpy)_2(bpy')]^{2+}/[Fe(bpy)_2(bpy')]^{3+}$ redox couple (Fig. 3), one could expect to regenerate the $[Fe(bpy)_2(bpy')]^{2+}$ species by the application of an appropriate potential (i.e. +0.5V). Upon applying +0.5 V to the working electrode for 1000s, one can observe a nearly 18% recovery of the MLCT absorption band of the $[Fe(bpy)_2(bpy')]^{2+}$ species, indicating that the process is only partial (Fig. S10). The incomplete recovery can be due to the rather long experiment time during which the immobilized complexes may suffer from poor stability (as reported for such species in solution[105,109,110]), consistent with multisweep CV results (Fig. 3B).

In a separate experiment, we have performed similar measurements, but recording the absorption at 525 nm (in the maximum of the MLCT absorption band) while varying the potential, by chronoamperometry technique (pulse amperometry), between 0 V and +1.3 V with a pulse of 10 s for each potential. The results are shown in figure 4. We can see that under these conditions, the switching between the redox states +2/+3 is achieved, with only a slight progressive decrease of the overall signal over the cycles.

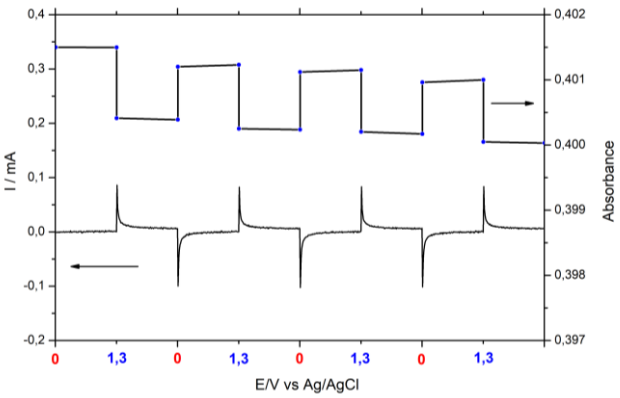

Figure 4. Variation of the absorbance of $[Fe(bpy)_2(bpy)]^{2+}$-functionalized films at a probe wavelength of 525 nm upon double step chronoamperometry between 0 and +1.3V (pulse width: 10 s).

To summarize, these experiments clearly show that it is indeed possible to control in a reversible way the optical properties of the nanocomposite thin film by the application of an external potential.

Light-induced electronic spin state change of the $[Fe(bpy)_2(bpy')]^{2+}$ functionalized films

Molecular Fe^{2+} spin-crossover systems are coordination complexes characterized by two low-lying electronic states of different spin multiplicities: the Low Spin (LS) state with electronic configuration ($^1A_1$, $t_{2g}^6e_g^0$, S=0) and the High Spin (HS) state with electronic configuration ($^5T_2$, $t_{2g}^4e_g^2$, S=2) in octahedral symmetry. The LS state is thermodynamically stable, while the HS state is thermally accessible at elevated temperature. In addition to this thermal spin-crossover, an efficient light-induced population of the HS state can be induced at very low temperature by irradiating into the spin allowed d-d bands, or the intense spin and dipole allowed metal to ligand charge transfer (MLCT) band of the LS species.[111] The general picture of this light-induced process has been revealed in the solvated as well as in the crystalline state by transient optical absorption, and X-ray pump-probe time resolved methods (X-ray diffraction and X-ray absorption spectroscopy).[112-124] In the general case, the initially excited state is extremely short-lived, and decays within less than a picosecond and with a near unity quantum yield non-radiatively to the HS state through a series of intermediate metal-centered (MC) or MLCT states by intersystem crossings. The subsequent metastable HS to ground state LS relaxation occurs through a non-adiabatic multiphonon process whose rate constant can be tuned chemically or physically.[125-128] In the solid state, the relaxation rate constant k_{HL} can in particular be heavily modified by internal or external pressure effects,[48] or modulated by the solute-solvent interactions in solution.[129,130]

For the specific case of $[Fe(bpy)_3]^{2+}$, owing to the large energy gap between the LS ground state and the lowest-lying HS state, the LS→HS transition in $[Fe(bpy)_3]^{2+}$ can only be triggered optically, and cannot be accessed thermally. As for the photo-induced behaviour, after excitation to the ^{1}MLCT manifold, the complex relaxes to the ^{3}MLCT state within 30 fs, from which it decays to the vibrationally hot $^5T_2$ state within 150 fs. The relaxation from the $^5T_2$ state to the $^1A_1$ LS ground state proceeds in 650 ps in aqueous solution at room temperature.[114,118] The intermediate ^{1}MLCT results from an electron transfer from the central Fe^{2+} ion to one of the three surrounding bpy ligand. During this process the Fe^{2+} ion is therefore oxidized to Fe^{3+}, while the transferred electron is strongly localized on one of the three bpy ligands. The formal charge distribution in the ^{1}MLCT state can by pictured $[Fe^{3+}(bpy^0)_2(bpy^-)]^{2+}$. As a consequence, the D_3 molecular symmetry is lowered to C_2, which has been proven by time-resolved Raman, and transient optical absorption spectroscopy for the $[Ru^{2+}(bpy)_3]^{2+}$ and $[Os^{2+}(bpy)_3]^{2+}$ analogues.[70,77,78,131] It has been shown that ligand substitution (for instance $[Fe(bpy)_3]^{2+}$ vs $[Fe(bpy)_2(CN)_2]^{2+}$ vs $[Fe(bpy)(CN)_4]^{2+}$) can lead to a modification of the whole photophysical behaviour, and in particular of the ordering of the excited state levels.[132,133] This means that the photophysics of such polypyridine complexes can be chemically tuned. The photocycle can be pictured as follows:

$$[Fe_{LS}^{2+}(bpy^0)_3]^{2+} \xrightarrow{h\nu} [Fe_{LS}^{3+}(bpy^0)_2(bpy^-)]^{2+} \xrightarrow{k_1} [Fe_{HS}^{2+}(bpy^0)_3]^{2+} \xrightarrow{k_{HL}} [Fe_{LS}^{2+}(bpy^0)_3]^{2+}$$

Where $[Fe_{LS}^{3+}(bpy^0)_2(bpy^-)]^{2+}$ is the photoexcited ^{1}MLCT state and $[Fe_{HS}^{2+}(bpy^0)_3]^{2+}$ is the quintet HS excited state. k_1 comprises the non-radiative decays and successive intersystem crossings to the HS excited state through intermediate triplet metal-centered or MLCT states, k_{HL} is the metastable state HS to ground state LS multiphonon relaxation rate.

In the context of our $[Fe(bpy)_2(bpy')]^{2+}$-functionalized silica films, the light induced LS-HS spin state change would offer a photomagnetic and photochromic functionality to the film associated to the large light-induced change of spin multiplicity ΔS=2. In order to verify this functionality, we have performed transient optical absorption measurements on the films. Let us recall that our sample consists of a mesoporous hydrated silica film deposited on an ITO electrode, and containing attached and confined $[Fe(bpy)_2(bpy')]^{2+}$ molecular species, so that, the $[Fe(bpy)_2(bpy')]^{2+}$ chromophores can be considered as solvated in a nanoscale environment. Using our optical setup, the time resolution is limited by the pump pulse duration of 4-5 ns, so that only the HS-LS relaxation step (of rate constant k_{HL}) of the whole photocycle can be captured. We used excitation light at 470 nm as pump pulse, and monitoring the kinetics of the absorption at 532 nm, corresponding to the maximum of the MLCT absorption of the LS ground state. The kinetics of the transient absorption spectrum at 532 nm is given in figure 5. We observe a process which overall lasts nearly 3 µs, and consists of several characteristic features. At first, the rapid decrease in absorbance corresponding to bleaching of the GS MLCT absorption band indicates the depopulation of the LS ground state and fast population of the metastable HS state. The absorption spectrum of the metastable HS state has been evaluated from the differential absorption spectrum by Brown et al. through transient optical absorption spectroscopy.[61] It shows a decrease in the MLCT absorption band which is due to a decrease of Metal-Ligand orbital overlap in the $^5T_2$ state, and therefore a decrease in charge transfer oscillator strength.[134,135] We have detected a similar trace for a 1 mM aqueous solution of $[Fe(bpy)_3]^{2+}$, with a time scale consistent with the measurement on the functionalized film (see Fig. S11), which confirms the assignment of this first step to the photo-induced LS→HS transition. After a few ns, the absorbance of the LS state is recovered, which corresponds to the HS-LS relaxation. One may argue that the relaxation occurs through a non-radiative multi-phonon relaxation mechanism, which is the dominant mechanism for Ru and OS similar complexes. The 1624 cm^{-1} skeleton vibration mode characterized in our static optical analysis is most probably the dominant deactivation mode involved in the HS→LS relaxation, which is consistent with literature results for the decay of charge transfer excited states in $[Ru(bpy)_3]^{2+}$ and $[Os(bpy)_3]^{2+}$.[136] Using our experimental resolution, the intermediate excited states (and especially the ^{1}MLCT state) are not detectable. The absorbance variation at longer time delay (viz. an increase of absorbance and further slow relaxation) corresponds to the characteristic behavior of the hydrated silica thin film, since we have measured a similar evolution on a neat non-functionalized hydrated film (see Fig. S12). We attribute this signal to a change of absorbance and reflectance of the mesoporous hydrated silica film after energy deposition following the pump 470 nm pulse. Thermal recovery occurs in the µs time scale.

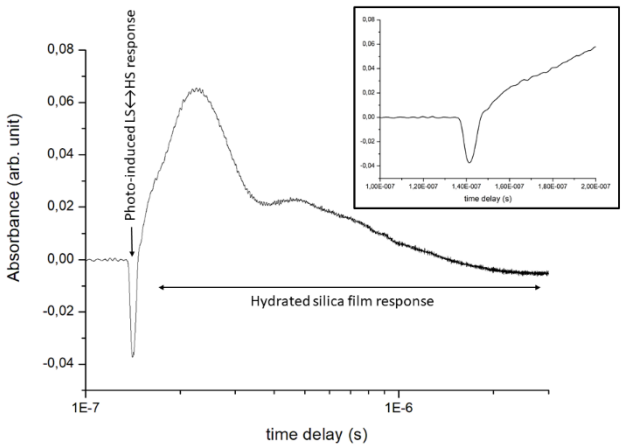

Figure 5. Kinetics of the UV-visible absorption data measured on $[Fe(bpy)_2(bpy')]$-functionalized films at 532nm (probe pulse) and excited at 470nm (pump pulse) in logarithmic scale (films prepared with 5% Az-PTES). Inset shows the signal at short time in linear scale.

If comparing the absorbance evolution within the first few ns between the aqueous solution and the silica film, although the absorption profile is pump pulse width limited, one can see a trend that the width in the film (fitted to 4.6ns) is lower than the width of the corresponding aqueous solution (5.1 ns) (this observation has been systematically reproduced on different films). This would indicate that the HS-LS relaxation is faster, and the HS state lifetime slightly shorter in the functionalized film

with respect to a $[Fe(bpy)_3]^{2+}$ aqueous solution. Such a different kinetics is not unexpected owing to the confined solvated environment of the $[Fe(bpy)_2(bpy')]^{2+}$ species in the mesoporous silica film. Several combined effects can influence this kinetics: a solvent effect, a local pressure/confinement effect, or a symmetry reduction induced by the bpy' chemical modification. Let's discuss these three possibilities hereafter.

The influence of the solvent in the photophysics of a solvated chromophore results from different parameters: change of dipole moment of the chromophore under light-induced electron-transfer, thermal solvent heating after energy deposition on the chromophore, solvent dynamical rearrangement and local density change, which all occur on different time scales. For $[Fe(bpy)_3]^{2+}$ and $[Ru(bpy)_3]^{2+}$, the initial ^{1}MLCT excited state exhibits a localization of the transferred electron on one of the three bpy ligands, inducing a strong molecular dipole moment. In a polar solvent, the resulting solute-solvent interactions can strongly modify the photophysical properties (non-radiative relaxation rate constants, luminescence energy and radiative relaxation rate constants).[129] In view of our experimental time resolution, this effect cannot be responsible for the observed increase of k_{HL} relaxation rate. Time-resolved diffuse X-ray scattering measurements have clearly quantified the solvent density change and temperature increase effects for solvated $[Fe(bpy)_3]^{2+}$.[132] It has been concluded that the solvent density change follows the same decay as the HS-LS relaxation, with a very similar time constant. In the case of our film, since the solvent is confined within the silica nanochannels, such a solvent density modification (or relaxation) is strongly restricted by the nanoconfined environment, which could possibly induce a local pressure on the light-induced HS $[Fe(bpy)_2(bpy')]^{2+}$ species. In the solid state, doping $[Fe(bpy)_3]^{2+}$ into a series of different inert crystalline hosts (thus generating different internal pressure) has revealed that the relaxation kinetics varies owing to the change in zero-point energy difference ΔE^0_{HL} ($\Delta E^0_{HL}=E^0_{HS}-E^0_{LS}$). Such a pressure effect results in a stabilization of the LS state, and therefore decrease of the HS state lifetime owing to the "inverse energy gap" law.[46,47] Time-resolved X-ray diffuse scattering has also shown that energy deposition from the pump pulse to the $[Fe(bpy)_3]^{2+}$ chromophore result in an increase of temperature on a longer time scale. Such a temperature increase would also result in a faster HS-LS relaxation in the functionalized films.

Formally, the chromophore attached to the inner walls of the mesoporous film is the heteroleptic $[Fe(bpy)_2(bpy')]^{2+}$ species, differing slightly from $[Fe(bpy)_3]^{2+}$ through a functionalization of one of the bpy ligand. This results in a symmetry lowering of the molecule from D_3 to C_2. It has been shown that a chemical functionalization of the bpy ligand, or ligand exchange may result in modifications of the corresponding photophysics.[132-133] In the present case, the effect of the chemical modification (bpy->bpy') may have an effect on the photophysics, but this effect is difficult to predict unambiguously.

A steric hindrance owing to the confined environment may also influence the photophysics of the $[Fe(bpy)_2(bpy')]^{2+}$-functionalized film. As a matter of fact, a modification of the molecular conformation has been concluded from resonance Raman measurements (Fig. 1). It has been shown that encapsulation of $[Fe(bpy)_3]^{2+}$, $[Ru(bpy)_3]^{2+}$, or $[Co(bpy)_3]^{2+}$ in zeolithic cavities may distort to some extent the chromophores,[137-140] resulting for instance in a spin crossover for the Co^{2+} complex,[139] or modified excited state lifetime and relaxation pathways for the Ru^{2+} complexes.[129,137,138] Such an encapsulation-induced distortion has been quantified by Vargas et al. from DFT calculations.[141]

As a conclusion, we may stress that our functionalized films do exhibit a light-induced $\Delta S=2$ spin state change, and therefore a photomagnetic response with a slight decrease of the excited state HS lifetime attributed to a combined effect of temperature increase and local solvent pressure increase, while a conformation and chemical modification of the chromophore may also play a role.

Generalization of the combined redox and light-induced switching capabilities

The method we followed to elaborate functionalized silica thin films containing covalently attached $[Fe(bpy)_2(bpy')]^{2+}$ entities using a combination of electro-assisted self-assembly methods and click chemistry reactions proved to be very efficient. It is well established that the transport phenomena through EASA prepared thin films is quite exceptional, much better than through thin films prepared by EISA or in non-templated thin films. In terms of confined complexation, the procedure consists in first attaching the bpy' ligand followed by sequential diffusion of Fe^{2+} and bpy. The approach is very versatile, so that mixed ligand complexes $[Fe(L)_2(bpy')]$ can be designed in a similar way.

The elaborated $[Fe(bpy)_2(bpy')]$-functionalized films present one-electron redox $[Fe^{2+}(bpy)_2(bpy')]^{2+}/[Fe^{3+}(bpy)_2(bpy')]^{3+}$ functionality leading to a reversible change of magnetic and optical properties. A further change of molecular spin multiplicity can be induced reversibly by light-excitation in the MLCT transition. The overall redox-control and light-induced control of the magnetic and optical properties of the $[Fe(bpy)_2(bpy')]$-functionalized film is illustrated in scheme 2. It is important to stress that the two functionalities exhibit very distinct response times. As demonstrated by the spectroelectrochemical analysis, the electrochemistry response time is quite slow, seconds time scale, while the light-induced spin crossover occurs on the nanoseconds time scale.

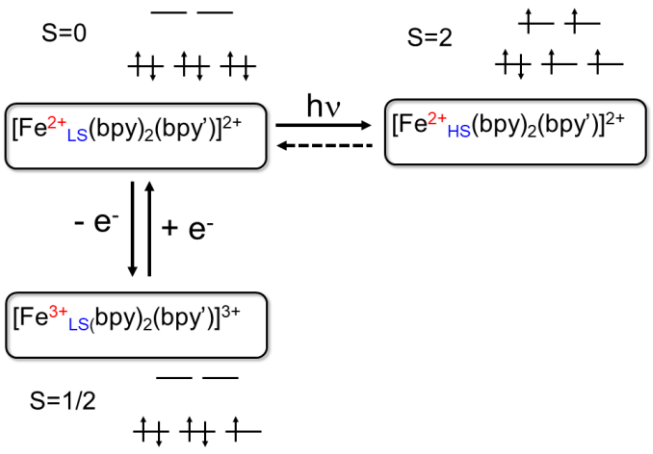

Scheme 2. Redox-control and light-induced control of the oxydation and spin state of the confined $[Fe(bpy)_2(bpy')]$ entity.

There is a close connection between the electrochemical and transient absorption properties of the $[Fe(bpy)_2(bpy')]^{2+}$ complex, both of which are directly related to the energy level diagram, and energy of the molecular frontier orbitals. DFT calculations based on geometry optimized structures report that the HOMO and LUMO molecular orbitals of the divalent $[Fe(bpy)_3]^{2+}$ complex consists of a metal-based HOMO, and ligand centered LUMO.[102] The oxidation of the complex involves removal of an electron from the highest occupied molecular orbital (HOMO) and is directly connected with the ionization potential ($IP=E_{complex}-E_{oxidized\ complex}$), while reduction involves the addition of an electron to the lowest unoccupied molecular orbital (LUMO) of the complex and is directly connected to the electron affinity.

Based on this analysis, the properties of the functionalized films could be tuned in several ways. At first, bpy ligands functionalized with electron donating or withdrawing functions could help at manipulating the respective positions of the HOMO and LUMO orbitals. For instance, shifting the HOMO to higher energy would lead to higher $E_{1/2}$ values since the ionization potential is increased. It has been observed for $M(bpy)_3$ derivatives, that strongly electron withdrawing (positive resulting shift of redox potential) or electron donating (negative resulting shift of redox potential) substituents on the bpy ligands can modify the wave position $E_{1/2}$ by as much as 1.5 V for Ru complexes,[87] and by more than 0.5 V for Fe complexes.[102] This offers a great opportunity to tune the electrochemical properties of the $[Fe(bpy)_2(bpy')]$-functionalized films by chemical design. The exchange of the bpy ligands by other ligands in the final impregnation step to form mixed ligand complexes $[Fe(L)_2(bpy')]$ can stabilize different oxidation states of the central coordinated metal, and therefore modify the whole molecular energy level diagram, especially the frontier orbitals, and as a consequence influence the potential of its redox reactions. The electronic excited state dynamics can be modified as well for mixed ligand complexes $[Fe(L)_2(bpy')]$. As an example, substitution of two bpy ligands by larger ligand field strength cyanide anions to form the complex $[Fe(CN)_4(bpy)]^{2-}$ enables the destabilization of the ligand field excited states while stabilizing the MLCT excited state, so that the lifetime of the MLCT excited state is much enhanced, and the HS-LS spin crossover is suppressed. As a consequence, the MLCT absorption is red-shifted for $[Fe(CN)_4(bpy)]^{2-}$ relative to $[Fe(bpy)_3]^{2+}$.

To summarize, the functionalized-thin films offer an unprecedented platform for tuning optical and magnetic properties of confined chromophores by chemical design.

Conclusion

A combination of electro-assisted self-assembly method and click chemistry reaction coupled with coordination chemistry allowed the design and elaboration of ordered and vertically oriented mesoporous silica thin films containing covalently attached $[Fe(bpy)_2(bpy')]^{2+}$ chromophores. According to TEM micrographs, the elaborated functionalized-films preserve their ordered and oriented mesoporosity. The vertical orientation of the silica framework proved to be efficient for fast molecular transport from/to the confined species through the films.

Measured cyclic voltammograms showed quasi reversible one-electron oxidation of the starting diamagnetic (S=0) $\left[Fe_{LS}(bpy)_2(bpy')\right]^{2+}$ cation to paramagnetic (S=1/2) $\left[Fe_{LS}(bpy)_2(bpy')\right]^{3+}$, leading to a possible redox control of the electronic properties of the functionalized films with ΔS=1/2 magnetic contrast. The change of oxidation state results at the same time in an electrochromic effect due to the partial bleaching of the metal-to-ligand charge transfer transition characteristic of the low spin $\left[Fe_{LS}(bpy)_2(bpy')\right]^{2+}$ species. The redox process is quite stable as steady-state voltammograms can be reached in multiple potential scanning.

Light absorption from the ground state dicationic species $\left[Fe_{LS}(bpy)_2(bpy')\right]^{2+}$ in the allowed MLCT transition leads to a very fast population of the metastable quintet (S=2) $\left[Fe_{HS}(bpy)_2(bpy')\right]^{2+}$ state through a succession of internal relaxation and intersystem crossings, as detected by transient absorption spectroscopy on the functionalized films. The lifetime of the metastable HS state is slightly shorter in the films with respect to aqueous solution, which is attributed to the combined effects of thermal solvent heating and pressure buildup on the confined $[Fe(bpy)_2(bpy')]^{2+}$ species.

Overall, the elaborated functionalized films present at the same time a redox control and an optical control of the electronic, optical and magnetic properties of the covalently attached and confined chromophores, which opens the field for their integration in smart optoelectronic devices.

Experimental Section

Chemicals and reagents

Tetraethoxysilane (TEOS, 98%, Alfa Aesar), ethanol (95-96%, Merck), HCl (37% Riedel de Haen), $NaNO_3$ (99%, Fluka), cetyltrimethylammonium bromide (CTAB, 99%, Acros) were used as received for films synthesis. 4,4′-dimethyl-2,2′-bipyridine (99%, Merck), sodium hydride (NaH, Merck, 90%), propargyl bromide (80 Wt.% solution in toluene, stabilized, ACROS organics), 1,4-dioxane (Merck, 99,8%), selenium (IV) oxide (SeO_2, ACROS organics, 99.8%), sodium carbonate (Na_2CO_3, Merck, 99.5%), sodium bicarbonate ($NaHCO_3$, Merck, 99%), magnesium sulfate anhydrous ($MgSO_4$, Merck, 99.5%), sodium chloride (Merck, 99.5%), methanol (Merck, 99.9%), dichloromethane (Merck, 99.8%) were analytical grade. $FeSO_4$ (Merck, 99%), 2,2'-bipyridine (bpy, Lancaster, 97%) lithium perchlorate ($LiClO_4$, Merck, 99.9%), (3-chloropropyl)triethoxysilane (95%, Sigma-Aldrich), sodium azide (NaN_3, 98% Sigma-Aldrich), tetrabutylammonium bromide (NBu_4Br, 99%, Sigma-Aldrich) and acetonitrile (CH_3CN, 99.9% Sigma-Aldrich) were used as received for the synthesis of the 3-azidopropyltriethoxysilane and the tris(2,2'-bipyridine) iron (II) sulfate.

Synthesis of (3-azidopropyl)triethoxysilane

(3-azidopropyl)triethoxysilane (AzPTES) was synthesized by reaction of ClPTES with NaN_3. ClPTES (2.0 g, 8.3 mmol) was added to a solution of NaN_3 (1.08 g, 16.6 mmol) and NBu_4Br (0.644 g, 2 mmol) in dry acetonitrile. The reaction mixture was stirred under reflux for 36 h. The mixture was cooled and the solvent evaporated under reduced pressure. The crude mixture was diluted in cyclohexane and the suspension was filtered. Solvent was removed from the resulting filtrate under reduced pressure at 70°C to give AzPTES as a crude oil. Yield: 1.33 g, 65%. 1H NMR (400 MHz, CDCl3): δ 0.66 (t, 2H, J = 0.85 Hz), 1.21 (t, 9H, J = 6.88 Hz), 1.66-1.73 (m, 2H), 3.25 (t, 2H, J = 7.16 Hz), m.80 (q, 6H, J = 6.88 Hz).

Synthesis of the 4-[(2-propyn-1-yloxy)]4'-methyl-2,2'-bypiridine (bpy')

The synthesis of 4-[(2-propyn-1-yloxy)]4'-methyl-2,2'-bypiridine was achieved in three steps starting from 4,4′-dimethyl-2,2′-bipyridine. In a first step 4,4′-dimethyl-2,2′-bipyridine was reacted with selenium oxide used as oxidizing agent in 1,4-dioxane to give the 4-(carboxyaldehyde)-4'-methyl-2,2'-bipyridine in good yields. The product was purified and isolated as previously described in the literature.[142] Subsequent chemical reduction of the carbaldehyde group was then performed using $NaBH_4$ in methanol reaching the corresponding 4-hydroxylmethyl-4'-methyl-2,2'-bipyridine. The last step consists of the deprotonation of the hydroxyl group by NaH followed by the addition of propargyl bromide in dry THF yielding the 4-[(2-propyn-1-yloxy)]4'-methyl-2,2'-bypiridine. 1H NMR (400 MHz, CDCl3) δ: 2.38 (s, 3H), 2.41 (t, J=2.4 Hz, 2H), 4.20 (d, J=2.4 Hz, 2H), 4.64 (s, 2H), 7.05-7.06 (m, 1H), 7.06-7.08 (m, 1H), 8.16-8.18 (m, 1H), 8.27-8.29 (m, 1H), 8.46 (d, J=5.0 Hz, 1H), 8.57 (d, J=5.0 Hz, 1H).

Synthesis of tris(2,2'-bipyridine) iron (II) sulfate, $[Fe(bpy)_3]SO_4.7.5H_2O$

Microcrystalline powder of $[Fe(bpy)_3]SO_4.7.5H_2O$ has been prepared as a reference material for the Raman spectroscopy investigations using a procedure previously reported.[143] 0.4 g of bpy was added to 20 ml of distilled water containing 0.1 g of $Fe(SO_4)$. The colourless aqueous solution turns to red when adding the 2,2'-bipyridyl characteristics of the formation of the $[Fe(bpy)_3]SO_4$ complex. The mixture is stirred for 15 to 20 min at room temperature. Thereafter, a few drops of 0.1 M $LiClO_4$ aqueous solution were added in order to promote the precipitation of the complex. The precipitate was recovered by filtration and dried in a desiccator.

Electrochemical experiments

All the electrochemical experiments were performed using a µAutoLab III potentiostat (Eco Chemie) monitored by the GPES software. A three-electrode configuration was employed in all cases, including the films electrogeneration and their characterization. The electrochemically-assisted deposition was carried out using a home-made electrochemical cell with a configuration allowing placing the working electrode at the bottom. A stainless-steel mesh was used as a counter electrode and a silver wire pseudo-reference electrode completed the electrochemical setup. The voltammetric curves were recorded using the working ITO plates covered with the hybrid films, a stainless-steel as counter-electrode and an Ag/AgCl reference electrode (Metrohm).

Spectroelectrochemistry measurements were carried out using a µAutoLab III potentiostat coupled with a UV-Vis spectrophotometer Carry 60. The $[Fe(bpy)_2(bpy')]^{2+}$-functionalized silica-based mesoporous films were placed in a quartz cell containing 0,1 M tetrabutylammonium tetrafluoroborate ($TBABF_4$) as electrolyte in acetonitrile. Two types of experiments were performed: (i) cyclic voltammetry curves were recorded while measuring the variation in optical absorbance through the film ; (ii) the wavelength of the spectrophotometer was fixed at 525 nm (corresponding to the characteristic MLCT absorption band, vide-supra) to monitor the variation of optical absorbance while performing chronoamperometry double step experiments (with consecutive oxidation and reduction pulses).

Preparation of the $[Fe(bpy)_2(bpy')]^{2+}$-functionalized mesoporous silica films

The hybrid mesoporous silica thin films have been prepared on ITO electrodes (surface resistivity 8-12 Ω) according to a procedure involving successively EASA, click coupling and complexation (scheme 1), in order to confine the chromophores in a covalently attached form ($[Fe(bpy)_2bpy')]^{2+}$) within the nanochannels.

In a first step ((a) in scheme 1), ordered and oriented azido-functionalized mesoporous silica films were prepared by co-condensation of TEOS and Az-PTES according to a slightly modified reported procedure.[19] A sol solution containing 190 mM TEOS and 10 mM AzPTES as silica precursors, and 64 mM CTAB as template in a concentration close to the critical micellar concentration, was prepared in hydroalcoholic medium (10 ml H_2O, 10 ml EtOH). $NaNO_3$ (0,1 M) was added as supporting electrolyte. The pH of the solution was adjusted to 3 by addition of an aqueous 0.1 M HCl solution and the sol was stirred at room temperature for 2.5 hours in order to hydrolyse the silica precursors. A cathodic potential of -1.3 V was applied during 20 s at the ITO working electrode dipped in this sol, to promote both the formation of hydroxyl ions by electrochemical reduction of water, necessary for polycondensation of the silica precursors, and at the same time induce the self-assembly of CTA^+ surfactant at the electrode surface.[12] The electrode was thoroughly rinsed with distilled water and ethanol, and kept at 130°C overnight to ensure good cross-linking of the silica network. The protocol described above refers to 5% AzPTES in the starting sol. The extraction of the surfactant CTAB was carried out by dipping the silica films in 0.1 M HCl in ethanol during 20 min.

In a second step ((b) in scheme 1), the azido-functionalized mesoporous silica films were derivatized with pendant 2-2'-bipyridine functions via an alkyne-azide Huisgen cycloaddition click-chemistry reaction, similarly as previously described for other triple-bonds bearing compounds (ethynylferrocene, ethynylcobaltocenium, propargyl-tetrazine, propargyl alcohol, pyridine).[19,20,22] For that purpose, we synthesized the {(4-[(2-propyn-1-yloxy)]4'-methyl-2,2'-bypiridine)} molecule (Scheme 1b, hereafter noted bpy') using a procedure described in the Supplementary Information. This bpy' derivative consists of an alkyne group substituted on a bipyridine entity, therefore appropriate for the envisioned cycloaddition click-chemistry reaction. The azido functionalized silica films deposited on ITO were dipped in the dark for 24 h in a solution of bpy' (9.4 mg), Cu(II) acetate (4 mg) and ascorbic acid (12 mg) in H_2O/DMF (6 ml / 14 ml). After this period, the films were dipped during 15 min in an ethanol solution of 0.05 M dithiocarbamate in order to remove traces of copper ions. The films were eventually rinsed in ethanol and dried.

The "ship in a bottle" complexation to form $[Fe(bpy)_2(bpy')]^{2+}$ was achieved by sequential complexation with Fe^{2+} and 2,2'-bipyridine species inside the silica mesochannels by successive impregnations of the film in $FeSO_4$ and bpy ((c) in scheme 1). The bpy' functionalized films were first dipped into a 10 mM $FeSO_4$ aqueous solution at pH = 6 for 2 hours under nitrogen atmosphere preventing Fe^{2+} to Fe^{3+} oxidation. The films were rinsed with acetonitrile, and subsequently dipped in a 30 mM 2,2'-bpy solution for 1 hour; the colour of the films turned from non-coloured to pink, characteristic of the presence of $[Fe(bpy)_2(bpy')]^{2+}$ complex inside the mesoporous matrix.

Physico-chemical measurements

Raman spectroscopy characterizations were performed using a confocal Raman microscope (inVia® Qontor with a Peltier-cooled CCD camera, Renishaw, Wotton-under-Edge, UK) equipped with a 532 nm laser (irradiance 50 kW cm^{-2}), a 50x objective with 0.55 of numerical aperture, and a 2400 lines.mm^{-1} grating. The spectral resolution was about 3 cm^{-1} (10 acquisitions of 4 seconds). Each sample was analyzed at different points to check the uniformity of the studied functionalized silica films. The laser power was optimized to 0.5 mW and the spectrum was recorded in the 50 to 4000 cm^{-1} wavenumber range.

The population and relaxation of light-induced short-lived excited states in the $[Fe(bpy)_2(bpy')]^{2+}$-functionalized films were measured using transient optical absorption spectroscopy with nanosecond time resolution following an optical pump-probe scheme. The thin film sample supported on ITO electrode was placed in a quartz cuvette, filled with distilled water playing the role of a cool bath for the dissipation of the optical energy deposited on the sample. The pump pulses were provided by a Surelite^{TM} Nd-YAG laser equipped with an OPO system tuned to λ=470 nm, with a pulse duration of t = 4-5 ns. The probe light was provided by a continuous laser centred at 532 nm and collected by a lens and focused to a spot size much smaller than the pump pulse in order to ensure proper overlap of the pump and probe pulses. The probe light was detected by a 200 MHz Si-Pin diode from Femto Messtechnik GmbH. The voltage at the output of the detector is sampled using a 1.5-GHz oscilloscope (Lecroy Wavepro 715zi). The optical absorption changes of the film induced by the photo-excitation was measured through the intensity change on the 200 MHz Si-Pin diode.

Mesostructure, morphology, and thickness of the films have been analyzed by transmission electron microscopy (TEM) using a ACCEL ARM 200F microscope at an acceleration voltage of 200 kV. X-ray Photoelectron Spectroscopy (XPS) characterizations were performed using a KRATOS Axis Ultra X-ray spectrometer (Kratos Analytical, Manchester, UK) equipped with a monochromated AlKα X-ray source (hv = 1486.6 eV) operated at 150 W.

Fourier transform infrared spectroscopy (FTIR) measurements were performed using a Nicolet 8700 apparatus in specular reflection condition.

Acknowledgements

We are grateful to the CNRS, the French PIA project "*Lorraine Université d'Excellence*" (reference ANR-15-IDEX-04-LUE), and the CPER (program *SusChemProc*), for financial supports. SA acknowledges a PhD fellow from the *Université de Lorraine*. We also thank Jaafar Ghanbaja for TEM imaging.

Keywords: Mesoporous silica • Thin film • Photo-switching • Redox-switching • Electrochemistry

[1] C. Sanchez, B. Julian, P. Belleville, M. Popall, *J. Mater. Chem*. **2005**, *15*, 3559.
[2] C. Sanchez, P. Belleville, M. Popall, L. Nicole, *Chem. Soc. Rev*. **2011**, *40*, 696.
[3] L. Nicole, C. Laberty-Robert, L. Rozes, C. Sanchez, *Nanoscale* **2014**, *6*, 6267.
[4] Y. Wan, D. Zhao, *Chem. Rev*. **2007**, *107*, 2821.
[5] P. Innocenzi, L. Malfatti, *Chem. Soc. Rev*. **2013**, *42*, 4198
[6] L. Nicole, C. Boissière, D. Grosso, A. Quach, C. Sanchez, *J. Mater. Chem*. **2005**, *15*, 3598.
[7] J. Cho, Y. Ishida, *Adv. Mater*. **2017**, *29*, 1605974.
[8] L. Mercier, T. j. Pinnavaia. *Adv. Mater*. **1997**, *9*, 500.
[9] A. Walcarius, M. Etienne, S. Sayen, B. Lebaeau, *Electroanalysis* **2003**, *15*, 414.
[10] D. Grosso, F. Cagnol, G. J. de A. A. Soler-Illia, E. L. Crepaldi, H. Amenitsch, A. Brunet-Bruneau, A. Bourgeois, C. Sanchez, *Adv. Funct. Mater.* **2004**, *14*, 309
[11] H. Yang, N. Coombs, I. Sokolov, G. A. Ozin, *Nature* **1996**, 381, 589.
[12] A. Walcarius, E. Sibottier, M. Etienne, J. Ghanbaja, *Nat. Mater*. **2007**, *6*, 602.
[13] A. Goux, M. Etienne, E. Aubert, C. Lecomte, J. Ghanbaja, A. Walcarius, *Chem. Mater*. **2009**, *21*, 731.
[14] G. Giordano, N. Vilà, E. aubert, J. Ghanbaja, A. Walcarius. *Electrochim. Acta* **2017**, *237*, 227.
[15] V. Urbanova, A. Walcarius, *Z. Anorg. Allg. Chem*. **2014**, *640*, 537.
[16] M. Etienne, A. Quach, D. Grosso, L. Nicole, C. Sanchez, A. Walcarius. *Chem. Mater*. **2007**, *19*, 844.
[17] M. Etienne, Y. Guillemin, D. Grosso, A. Walcarius. *Anal. Bioanal. Chem*. **2013**, *405*, 1497.
[18] D. Feng, J. Wei, M. Wang, Q. Yue, Y. Deng, A. M. Asiri, D. Zhao, *Adv. Porous Mater*. **2013**, *1*, 164.
[19] N. Vilà, J. Ghanbaja, E. Aubert, A. Walcarius, *Angew. Chem. Int. Ed*. **2014**, *53*, 2945.
[20] N. Vilà, J. Ghanbaja, A. Walcarius, *Adv. Mater. Interfaces* **2016**, *3*, 1500440.
[21] P. Audebert, N. Vilà, C. allain, F. Maisonneuve, A. Walcarius, P. Hapiot, *ChemElectroChem*. **2015**, *2*, 1695.
[22] N. Vilà, C. Allain, P. Audebert, J. Ghanbaja, A. Walcarius. *Electrochem. Commun.* **2015**, *59*, 9.
[23] C. Wang, M. Amiri, R. T. Endean, O. M. Perez, S. Varley, B. Rennie, L. Rasu, S. H. Bergens, *ACS Appl. Mater. Interfaces* **2018**, *10*, 24533.
[24] J. Font, P. de March, F. Busqué, E. Casas, M. Benitez, L. Teruel, H. Garcia, *J Mater. Chem*. **2007**, *17*, 2336.
[25] H. Zhang, B. Li, B. Lei, W. Li, S. Lu, *Sens. Actuators B Chem.* **2007**, *123*, 508.
[26] A. Quach, V. Escax, L. Nicole, P. Goldner, O. Guillot-Noël, P. Aschehoug, P. Hesemann, J. Moreau, D. Gourier, C. Sanchez, *J. Mater. Chem*. **2007**, *17*, 2552.
[27] M. Sohmiya, Y. Sugahara, M. Ogawa, *J. Phys. Chem. B* **2007**, *111*, 8836.
[28] P. Innocenzi, H. Kozuka, T. Yoko, *J. Phys. Chem. B* **1997**, *101*, 2285.
[29] D. Brühwiler, G. Calzaferri, T. Torres, J. H. Ramm, N. Gartmann, L.-Q. Dieu, I. Lopez-Duarte, M. V. Martinez-Diaz, *J. Mater. Chem*. **2009**, *19*, 8040.
[30] M. Tan, Q. Liu, S. yang, Y. Gu, B. Zhu, Y. Cao, Y. Gao, *Mater. Lett.* **2017**, *209*, 589.
[31] T. Nasir, G. Herzog, M. Hebrant, C. Despas, L. Liu, A. Walcarius, *ACS Sens.* **2018**, *3*, 484.
[32] Y. Ali, H. Smida, J. Ghilane, N. Vila, J. Ghanbaja, A. Walcarius, J. C. Lacroix, *Sci. Rep.* **2017**, *7*, 17752.
[33] H. Luo, D. Wang, J. He, Y. Lu, *J. Phys. Chem. B* **2005**, *109*, 1919.
[34] W. Cui, X. Lu, B. Su, Q. Lu, Y. Wei, *Appl. Phys. Lett*. **2009**, *95*, 153102.
[35] W. C. Molenkamp, M. Watanabe, H. Miyata, S. H. Tolbert, *J. Am. Chem. Soc*. **2004**, *126*, 4476.
[36] A. Fukuoka, H. Miyata, K. Kuroda, *Chem. Commun*. **2003**, 284.
[37] F. Shan, X. Lu, Q. Zhang, B. Su, Q. Lu, *Langmuir* **2011**, *28*, 812.
[38] S. Ahoulou, N. Vilà, S. Pillet, D. Schaniel, A. Walcarius, *Chem. Mater*. **2019**, 31, 5796.
[39] G. M. Greenway, A. Greenwood, P. Watts, C. Wiles, *Chem. Commun*. **2006**, 85.
[40] M. K. Nazeeruddin, C. Klein, P. Liska, M. Graetzel, *Coord. Chem. Rev*. **2005**, *249*, 1460.
[41] F. G. Gao, A. J. Bard, *J. Am. Chem. Soc*. **2000**, *122*, 7426
[42] S. H. Bossmann, S. Jockusch, P. Schwarz, B. Baumeister, S. Gob, C. Schnabel, L. Payawan, M. R. Pokhrel, M. Worner, A. M. Braun, N. J. Turro, *Photochem. Photobiol. Sci*. **2003**, *2*, 477.
[43] J. Mun, M-J. Lee, J.-W. Park, D.-J. Oh, D.-Y Lee, S.-G. Doo, *Electrochem. Solid State Lett*. **2012**, *15*, A80.
[44] G. M. Duarte, J. D. Braun, P. K. Giesbrecht, D. E. Herbert, *Dalton Trans*. **2017**, *46*, 16439.
[45] A. Hauser, *Chem. Phys. Lett*. **1990**, *173*, 507.
[46] A. Hauser, A. Vef, P. Adler, *J. Chem. Phys*. **1991**, *95*, 8710.
[47] S. Schenker, A. Hauser, W. Wang, I. Y. Chan, *Chem. Phys. Lett*. **1998**, *297*, 281.
[48] A. Hauser, C. Enachescu, M. Lawson Daku, A. Vargas, N. Amstutz, *Coord. Chem. Rev*. **2006**, *250*, 1642.
[49] K. S. Kjaer, T. B. Van Driel, T. C. B. Harlang, K. Kunnus, E. Biasin, K. Ledbetter, R. W. Hartsock, M. E. Reinhard, S. Koroidov, L. Li, M. G. Laursen, F. B. Hansen, P. Vester, M. Christensen, K. Haldrup, M. M. Nielsen, A. O. Dohn, M. I. Papai, K. B. Moller, P. Chabera, Y. Liu, H. Tatsuno, C. Timm, M. Jarenmark, J. Uhlig, V. Sundstom, K. Warnmark,

P. Persson, Z. Nemeth, D. S. Szemes, E. Bajnoczi, G. Vanko, R. Alonso-Mori, J. M. Glownia, S. Nelson, M. Sikorski, D. Sokaras, S. E. Canton, H. T. Lemke, K. J. Ganney, *Chem. Sci*. **2019**, *10*, 5749.

[50] H. T. Lemke, Ch. Bressler, L. X. Chen, D. M. Fritz, K. J. Gaffney, A. Galler, W. Gawelda, K. Haldrup, R. W. Hartsock, H. Ihee, J. Kim, K. H. Kim, J. H. Lee, M. N. Nielsen, A. B. Stickrath, W. Zhang, D. Zhu, M. Cammarata, *J. Phys. Chem. A*. **2013**, *117*, 735.

[51] W. Gawelda, V.-T. Pham, M. Benfatto, Y. Zaushitsyn, M. Kaiser, D. Grolimund, S. L. Johson, R. Abela, A. Hauser, Ch. Bressler, M. Chergui, *Phys. Rev. Lett*. **2007**, *98*, 057401.

[52] Ch. Bressler, C. Milne, V.-T. Pham, A. ElNahhas, R. M. van der Veen, W. Gawelda, S. Johnson, P. Beaud, D. Grolimund, M. Kaiser, C. N. Borca, G. Ingold, R. Abela, M. Chergui., *Science* **2009**, *323*, 489.

[53] A. Cannizzo, C. J. Milne, C. Consani, W. Gawelda, Ch. Bressler, F. van Mourik, M. Chergui, *Coord. Chem. Rev*. **2010**, *254*, 2677.

[54] J. E. Monat, J. K. McCusker, *J. Am. Chem. Soc*. **2000**, *122*, 4092.

[55] M. C. Carey, S. L. Adelman, J. K. McCusker, *Chem. Sci*. **2019**, *10*, 134.

[56] W. Gawelda, A. Cannizzo, V.-T. Pham, F. van Mourik, C. Bressler, M. Chergui, *J. Am. Chem. Soc*. **2007**, *129*, 8199.

[57] A. Cannizzo, F. van Mourik, W. Gawelda, G. Zgrablic, C. Bressler, M. Chergui, *Angew. Chem. Int. Ed*. **2006**, *45*, 3174.

[58] J. K. McCusker, K. N. Walda, R. C. Dunn, J. D. Simon, D. Magde, D. N. Hendrickson, *J. Am. Chem. Soc*. **1993**, *115*, 298.

[59] J. K. McCusker, K. N. Walda, R. C. Dunn, J. D. Simon, D. Magde, D. N. Hendrickson, *J. Am. Chem. Soc*. **1992**, *114*, 6919.

[60] G. Aubock, M. Chergui, *Nat. Chem*. **2015**, *7*, 629.

[61] A. M. Brown, C. E. McKusker, J. K. McCusker, *Dalton Trans*. **2014**, *43*, 17635.

[62] M. A. Bergkamp, C.-K. Chang, T. L. Netzel, *J. Phys. Chem*. **1983**, *87*, 4441.

[63] O. Sato, J. Tao, Y.-Z. Zhang, *Angew. Chem. Int. Ed*. **2007**, *46*, 2152-2187.

[64] O. Sato, *Nat. Chem.* **2016**, *8*, 644-656.

[65] Z.-S. Yao, Z. Tang, J. Tao, *Chem. Commun*. **2020**, *56*, 2071-2086.

[66] N. Vilà, A. Walcarius. *Front. Chem.* **2020**, *8*, 830.

[67] R. M. Almeida, C. G. Pantano, *J. Appl. Phys*. **1990**, *68*, 4225.

[68] E. I. Kamitsos, A. Patsis, G. Kordas, *Phys. Rev*. **1993**, *B48*, 12499

[69] E. Lieber, C. N. Ramachandra Rao, T. S. Chao, C. W. W. Hoffman, *Anal. Chem.* **1957**, *29*, 916.

[70] D. P. Strommen, P. K. Mallick, G. D. Danzer, R. S. Lumpkin, J. R. Kincaid, *J. Phys. Chem*. **1990**, *94*, 1357.

[71] D. S. Caswell, T. G. Spiro, *Inorg. Chem*. **1987**, *26*, 18.

[72] P. K. Mallick, G. D. Danzer, D. P. Strommen, J. R. Kincaid, *J. Phys. Chem.* **1988**, *92*, 5628.

[73] T. J. Dines, R. D. Peacock, *J. Chem. Soc., Faraday Trans*. **1988**, *84*, 3445.

[74] R. M. Berger, D. R. McMillin, *Inorg. Chim. Acta*, **1990**, *177*, 65.

[75] B. D. Alexander, T. J. Dines, R. W. Longhurst, *Chem. Phys*. **2008**, *352*, 19.

[76] B. Hutchinson, J. Takemoto, K. Nakamoto, *J. Am. Chem. Soc*. **1970**, *92*, 3335.

[77] P. G. Bradley, N. Kress, B. A. Hornberger, R. F. Dallinger, W. H. Woodruff, *J. Am. Chem. Soc*. **1981**, *103*, 7441.

[78] P. J. Carroll, L. E. Brus, *J. Am. Chem. Soc*. **1987**, *109*, 7613.

[79] V. V. Avdeeva, A. V. Vologzhanina, L. V. Goeva, E. A. Malinina, N. T. Kuznetsov, *Z. Anorg. Allg. Chem*. **2014**, *640*, 2149.

[80] R. J. H. Clark, P. C. Turtle, D. P. Strommen, B. Steusand, J. Kincaid, K. Nakamoto, *Inorg. Chem*. **1977**, *16*, 84.

[81] P. J. Miller, R. S.-L. Chao, *J. Raman Spectr*. **1979**, *8*, 17.

[82] J. S. Strukl, J. L. Walter, *Spectrochim. Acta* **1971**, *27A*, 209.

[83] Y. Saito, J. Takemoto, B. Hutchinson, K. Nakamoto, *Inorg. Chem*. **1972**, *11*, 2003.

[84] A. Bousseksou, J. J. McGarvey, F. Varret, J. A. Real, J.-P. Tuchagues, A. C. Deniis, M. L. Boillot, *Chem. Phys. Lett*. **2000**, *318*, 409

[85] J. H. Takemoto, B. Hutchinson, *Inorg. Chem*. **1973**, *12*, 705.

[86] E. König, K. Madeja, K. J. Watson, *J. Am. Chem. Soc*. **1968**, *90*, 1146.

[87] D. van der Westhuizen, K. G. von Eschwege, J. Conradie, *Electrochim. Acta* **2019**, *320*, 134540.

[88] J. P. Tuchagues, A. Bousseksou, G. Molnar, J. J. McGarvey, F. Varret, in *Top. Curr. Chem*. *Vol. 235* (Eds P. Gütlich, H. A. Goodwin), **2004**, pp. 85-103.

[89] M. Konno, M. Mikami-Kido, *Bull. Chem. Soc. Jpn*, **1991**, *64*, 339.

[90] C. M .Elliott, S. Caramori, C. A. BignozziLangmuir 2005, 21, 3022-3027.

[91] D. Moulin Cabral, P. C. Howlett, D. R. MacFarlane, *Electrochim. Acta*, **2016**, *220*, 347.

[92] Allen J. Bard and Larry R. Faulkner, *Electrochemical Methods: Fundamentals and Applications* (2nd ed.) John Wiley & Sons **2001**.

[93] N. Vilà, A. Walcarius, *Electrochim. Acta* **2015**, *179*, 304.

[94] J. V. Caspar, T. J. Meyer, *Inorg. Chem*. **1983**, *22*, 2444.

[95] C. Creutz, M. Chou, T. L. Netzel, M. Okumura, N. Sutin, *J. Am. Chem. Soc*. **1980**, *102*, 1309.

[96] E. M. Kober, B. P. Sullivan, T. J. Meyer, *Inorg. Chem*. **1984**, *23*, 2098.

[97] R. A. Palmer, T. S. Piper, *Inorg. Chem*. **1966**, *5*, 864.

[98] F. Felix, J. Ferguson, H. U. Gudel, A. Ludi, *J. Am. Chem. Soc*. **1980**, *102*, 4096.

[99] S. Decurtins, F. Felix, J. Ferguson, H. U. Guel, A. Ludi, *J. Am. Chem. Soc*. **1980**, *102*, 4102.

[100] J. Ferguson, F. Herren, *Chem. Phys. Lett*. **1982**, *89*, 371.

[101] J. Ferguson, F. Herren, *Chem. Phys*. **1983**, *76*, 45.

[102] H. Ferreira, K. G. von Eschwege, J. Conradie, *Electrochim. Acta* **2016**, *216*, 339.

[103] A. Ceulemans, L. G. Vanquickenborne, *J. Am. Chem. Soc*. **1981**, *103*, 2238.

[104] H. Yersin, E. Gallhuber, G. Hensler, *Chem. Phys. Lett*. **1987**, *134*, 497.

[105] S. Sahami, R. A. Osteryoung, *Inorg. Chem.* **1984**, *23*, 2511.

[106] J. G. Gaudiello, P. R. Sharp, A. J. Bard, *J. Am. Chem. Soc*. **1982**, *104*, 6373.

[107] C. L. Wong, J. K. Kochi, *J. Am. Chem. Soc*. **1979**, *101*, 5593.

[108] G. M. Bryant, J. E. Fergusson, *Aust. J. Chem*. **1971**, *24*, 275.

[109] N. Tanaka, Y. Sato, *Electrochim. Acta* **1968**, *13*, 335.

[110] Y.W. D. Chen, K. S. V. Santhanam, A. J. Bard, *J. Electrochem. Soc*. **1981**, *128*, 1460.

[111] P. Gütlich, H. A. Goodwin, eds, *Top. Curr. Chem. 233-235*, Springer, Heidelberg, **2004**.

[112] K. S. Kjaer, T. B. Van Driel, T. C. B. Harlang, K. Kunnus, E. Biasin, K. Ledbetter, R. W. Hartsock, M. E. Reinhard, S. Koroidov, L. Li, M. G. Laursen, F. B. Hansen, P. Vester, M. Christensen, K. Haldrup, M. M. Nielsen, A. O. Dohn, M. I. Papai, K. B. Moller, P. Chabera, Y. Liu, H. Tatsuno, C. Timm, M. Jarenmark, J. Uhlig, V. Sundstom, K. Warnmark, P. Persson, Z. Nemeth, D. S. Szemes, E. Bajnoczi, G. Vanko, R. Alonso-Mori, J. M. Glownia, S. Nelson, M. Sikorski, D. Sokaras, S. E. Canton, H. T. Lemke, K. J. Ganney, *Chem. Sci*. **2019**, *10*, 5749.

[113] H. T. Lemke, Ch. Bressler, L. X. Chen, D. M. Fritz, K. J. Gaffney, A. Galler, W. Gawelda, K. Haldrup, R. W. Hartsock, H. Ihee, J. Kim, K. H. Kim, J. H. Lee, M. N. Nielsen, A. B. Stickrath, W. Zhang, D. Zhu, M. Cammarata, *J. Phys. Chem. A*. **2013**, *117*, 735.

[114] W. Gawelda, V.-T. Pham, M. Benfatto, Y. Zaushitsyn, M. Kaiser, D. Grolimund, S. L. Johson, R. Abela, A. Hauser, Ch. Bressler, M. Chergui, *Phys. Rev. Lett*. **2007**, *98*, 057401.

[115] Ch. Bressler, C. Milne, V.-T. Pham, A. ElNahhas, R. M. van der Veen, W. Gawelda, S. Johnson, P. Beaud, D. Grolimund, M. Kaiser, C. N. Borca, G. Ingold, R. Abela, M. Chergui., *Science* **2009**, *323*, 489.

[116] A. Cannizzo, C. J. Milne, C. Consani, W. Gawelda, Ch. Bressler, F. van Mourik, M. Chergui, *Coord. Chem. Rev*. **2010**, *254*, 2677.

[117] J. E. Monat, J. K. McCusker, *J. Am. Chem. Soc*. **2000**, *122*, 4092.

[118] M. C. Carey, S. L. Adelman, J. K. McCusker, *Chem. Sci*. **2019**, *10*, 134.

[119] W. Gawelda, A. Cannizzo, V.-T. Pham, F. van Mourik, C. Bressler, M. Chergui, *J. Am. Chem. Soc*. **2007**, *129*, 8199.

[120] A. Cannizzo, F. van Mourik, W. Gawelda, G. Zgrablic, C. Bressler, M. Chergui, *Angew. Chem. Int. Ed*. **2006**, *45*, 3174.

[121] J. K. McCusker, K. N. Walda, R. C. Dunn, J. D. Simon, D. Magde, D. N. Hendrickson, *J. Am. Chem. Soc*. **1993**, *115*, 298.

[122] J. K. McCusker, K. N. Walda, R. C. Dunn, J. D. Simon, D. Magde, D. N. Hendrickson, *J. Am. Chem. Soc*. **1992**, *114*, 6919.

[123] G. Aubock, M. Chergui, *Nature Chem*. **2015**, *7*, 629.

[124] A. M. Brown, C. E. McKusker, J. K. McCusker, *Dalton Trans*. **2014**, *43*, 17635.

[125] A. Hauser, *Chem. Phys. Lett*. **1986**, *124*, 543.
[126] A. Hauser, *J. Chem. Phys*. **1991**, *94*, 2741.
[127] A. Hauser, P. Gutlich, H. Spiering, *Inorg. Chem*. **1986**, *25*, 4245.
[128] A. Hauser, J. Jeftic, H. Romstedt, R. Hinek, H. Spiering, *Coord. Chem. Rev*. **1999**, *190-192*, 471.
[129] P.Innocenzi, H. Kozuka, T. Yoko, *J. Phys. Chem. B* **1997**, *101*, 2285.
[130] K. S. Kjaer, K. Kunnus, T. C. B. Harlang, T. B. Van Driet, K. Ledbetter, R. W. Hartsock, M. E. Reinhardt, S. Koroidov, L. Li, M. G. Laursen, E. Biasin, F. B. Hansen, P. Vester, M. Christensen, K. Haldrup, M. M. Nielsen, P. Chabera, Y. Liu, H. Tatsuno, C. Timm, J. Uhlig, V. Sundstom, Z. Nemeth, D. S. Szemes, E. Bajnoczi, G. Vanko, R. Alonso-Mori, J. M. Glownia, S. Nelson, M. Sikorski, D. Sokaras, H. T. Lemke, S. E. Canton, K. Warnmark, P. Persson, A. A. Cordones, K. J. Gaffney, *Phys. Chem. Chem. Phys*. **2018**, *20*, 4238.
[131] P. S. Braterman, A. Harriman, G. A. Heath, L. J. Yellowlees, *J. Chem. Soc. Datlon Trans*. **1983**, 1801.
[132] W. Zhang, K. S. Kjaer, R. Alonso-Mori, U. Bergmann, M. Chollet, L. A. Fredin, R. G. Hadt, R. W. Hartsock, T. Harlang, T. Kroll, K. Kubicek, H. T. Lemke, H. W. Liang, Y. Liu, M. M. Nielsen, P. Persson, J. S. Robinson, E. I. Solomon, Z. Sun, D. Sokaras, T. B. van Driel, T.-C. Weng, D. Zhu, K. Warnmark, V. Sundstrom, K. J. Gaffney, *Chem. Sci*. **2017**, *8*, 515.
[133] K. S. Kjaer, W. Zhang, R. Alonso-Mori, U. Bergmann, M. Chollet, R. G. Hadt, R. W. Hartsock, T. Harlang, T. Kroll, K. Kubicek, H. T. Lemke, H. W. Liang, Y. Liu, M. M. Nielsen, J. S. Robinson, E. I. Solomon, D. Sokraras, T. B. van Driel, T.-C. Weng, D. Zhu, P. Persson, K. Warnmark, V. Sundstrom, K. J. Gaffney, *Struct. Dyn*. **2017**, *4*, 044030.
[134] S. M. Angel, M. K. DeArmond, R. J. Donohoe, K. W. Hanck, D. W. Wertz, *J. Am. Chem. Soc*. **1984**, *106*, 3688.
[135] A. L. Smeigh, M. Creelman, R. A. Mathies, J. K. McCusker, *J. Am. Chem. Soc*. **2008**, *130*, 14105.
[136] J. V. Caspar, E. M. Kober, B. P. Sullivan, T. J. Meyer, *J. Am. Chem. Soc*. **1982**, *104*, 630.
[137] K. Maruszewski, J. R. Kincaid, *Inorg. Chem*. **1995**, *34*, 2002.
[138] G. Sewell, R. J. Forster, T. E. Keyes, *J. Phys. Chem. A* **2008**, *112*, 880.
[139] K. Mizuno, J. H. Lunsford, *Inorg. Chem*. **1983**, *22*, 3484.
[140] R. Vijayalakshmi, S. K. Kulshreshtha, *Microporous Mesoporous Mater.* **2008**, *111*, 449.
[141] A. Vargas, A. Hauser, L. Max Lawson Daku, *J Chem. Theory, Comput*. **2009**, *5*, 97.
[142] A. Walcarius, R. Nasraoui, Z. Wang, F. Qu, V. Urbanova, M. Etienne, M. Göllü, A. Demir, J. Gajdzik, R. Hempelmann, *Bioelectrochemistry* **2011**, *82*, 46.
[143] J. K. Mccusker, K. N. Walda, R. C. Dunn, J. D. Simon, D. Magde, D. Hendrickson. *J. Am. Chem. Soc*. **1993**, *115*, 298.

Entry for the Table of Contents

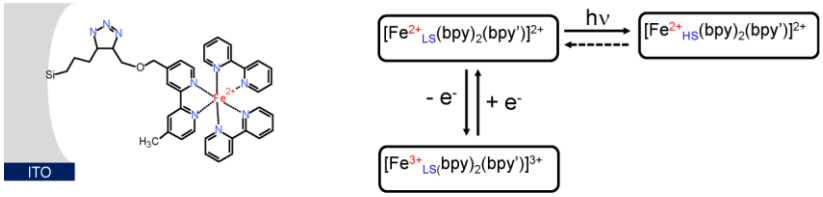

Fe(btr)$_3$-functionalized silica films, which show at the same time a redox control and an optical control of the electronic, optical and magnetic properties of the covalently attached and confined chromophores, are presented. The films show a quasi-reversible one-electron oxidation of the diamagnetic (S=0) confined cation to paramagnetic (S=1/2) under redox control, while light excitation leads to a low spin (S=0) to high spin (S=2) transition.